

# Quantum chemistry beyond Born-Oppenheimer approximation on a quantum computer: a simulated phase estimation study

Libor Veis<sup>\*,†</sup>, Jakub Višňák<sup>\*,†</sup>, Hiroaki Nishizawa<sup>‡</sup>, Hiromi Nakai<sup>§</sup>, Jiří Pittner<sup>†</sup>

March 5, 2022

## Abstract

We present an *efficient* quantum algorithm for beyond-Born-Oppenheimer molecular energy computations. Our approach combines the quantum full configuration interaction method with the nuclear orbital plus molecular orbital (NOMO) method. We give the details of the algorithm and demonstrate its performance by classical simulations. Two isotopomers of the hydrogen molecule ( $\text{H}_2$ , HT) were chosen as representative examples and calculations of the lowest rotationless vibrational transition energies were simulated.

---

<sup>\*</sup>These authors contributed equally.

<sup>†</sup>J. Heyrovský Institute of Physical Chemistry, Academy of Sciences of the Czech Republic, v.v.i., Dolejškova 3, 18223 Prague 8, Czech Republic

<sup>‡</sup>Present address: Institute for Molecular Science, 38 Nishigo-Naka, Myodaiji, Okazaki, 444-8585, Japan

<sup>§</sup>Department of Chemistry and Biochemistry, School of Advanced Science and Engineering, Waseda University, 3-4-1 Okubo, Shinjuku, Tokyo 169-8555, Japan

# 1 Introduction

Exact computations and simulations of quantum systems on a classical computer are computationally hard. This stems from the fact that the dimensionality of the Hilbert space needed for the description of a studied quantum system scales exponentially with its size. One of the consequences is e.g. the prohibitive exponential scaling of the full configuration interaction (FCI) method. Quantum computers<sup>1</sup>, on the other hand, offer an exponential speed-up for this task<sup>2-8</sup>, as was first noticed by Feynman and Manin<sup>9,10</sup>. The underlying idea, which employs mapping of the Hilbert space of a studied quantum system onto the Hilbert space of a register of quantum bits (qubits), both of them being exponentially, large, can in fact be adopted also in quantum chemistry.

The past few years have witnessed a remarkable interest in the application of quantum computing for solving of different problems in quantum chemistry. Among others, quantum algorithms for non-relativistic<sup>11-14</sup> as well as relativistic<sup>15</sup> molecular FCI energy calculations, quantum chemical dynamics<sup>16</sup>, or calculations of molecular properties<sup>17</sup> were developed. For a complete list of relevant papers, we refer the reader to recent reviews<sup>18-20</sup>. *Efficient* quantum chemical simulations are indeed believed to belong to the first practical applications of quantum computers. This is also supported by recent proof-of-principle few-qubit experiments<sup>21-26</sup>. Several improvements reducing the resource requirements of fault-tolerant implementation and thus paving the way for practical simulations were presented in<sup>27</sup>.

In this paper, motivated by the fact that non-Born-Oppenheimer (non-BOA) effects play an essential role in wide range fields (e.g. proton tunnelling in DNA damage), we generalise the applicability of the quantum FCI algorithm<sup>11,13</sup> for beyond-BOA computations. We achieve this by combining qFCI with the NOMO method<sup>28-34</sup>. We should however note that our attempt is not the first one dealing with beyond-BOA computations on a quantum computer. In<sup>16</sup>, it was shown that simulating all electron-nuclear and inter-electronic interactions (and thus going beyond BOA) is somewhat surprisingly faster and more efficient than BOA for systems with more than four atoms. Nevertheless, the aforementioned approach is based on the first quantized formulation, thus completely different from ours.

The structure of the paper is following. In Section 2 we shortly review the basic concepts of the phase estimation-based quantum FCI algorithm<sup>11,13</sup>, in Section 3 we do the same for the NOMO method, and in Section 4 we present details of our quantum algorithm for beyond-BOA computations, which is a combination of both approaches. The performance of the proposed scheme is presented in Section 5 by classical simulations of H<sub>2</sub> and HT energy computations.

## 2 Quantum FCI algorithm

An *efficient* quantum FCI (qFCI) algorithm for calculations of nonrelativistic molecular energies employing the phase estimation algorithm (PEA) of Abrams and Lloyd<sup>7</sup> was proposed in the pioneering work by Aspuru-Guzik *et al.*<sup>11</sup>. It was later simplified by replacing of PEA with its iterative version, iterative phase estimation algorithm (IPEA)<sup>12-14</sup>. (I)PEA is a quantum algorithm for obtaining the eigenvalue of a unitary operator  $\hat{U}$ , based on a given initial guess of the corresponding eigenvector. Since a unitary  $\hat{U}$  can be written as  $\hat{U} = e^{i\hat{H}}$ , with  $\hat{H}$  Hermitian, the (I)PEA can be viewed as a quantum substitute of the classical diagonalization.

Suppose that  $|u\rangle$  is an eigenvector of  $\hat{U}$  and that it holds

$$\hat{U}|u\rangle = e^{2\pi i\phi}|u\rangle, \quad \phi \in (0, 1), \quad (1)$$

where  $\phi$  is the phase which is estimated by the algorithm. In case of the original PEA, a quantum

register is divided into two parts. The first one is the read-out part composed of  $m$  qubits on which the binary representation of the estimate of phase  $\phi$  is eventually measured. After the application of Hadamard gates in the read-out part of the quantum register followed by application of a sequence of controlled- $\hat{U}^{2^{k-1}}$  operations ( $k$ s are nonnegative integers from 1 to  $m$ ), the register is transformed into

$$|\text{reg}\rangle = \frac{1}{\sqrt{2^m}} \sum_{j=0}^{2^m-1} \hat{U}^j |j\rangle |u\rangle = \frac{1}{\sqrt{2^m}} \sum_{j=0}^{2^m-1} e^{2\pi i j \phi} |j\rangle |u\rangle. \quad (2)$$

The next part of the algorithm is the inverse quantum Fourier transform (QFT)<sup>1</sup> performed on the read-out part of the register. The whole register is transformed into  $|2^m \phi\rangle |u\rangle$  and the phase can be extracted from its first part.

Iterative version, IPEA adopts the ideas of measurement-based quantum computing<sup>35</sup> and reduces the computational resources by using only single read-out qubit. If  $\phi$  is expressed in the binary form:  $\phi = 0.\phi_1\phi_2\dots\phi_m$ ,  $\phi_i = \{0, 1\}$ , one bit of  $\phi$  is measured on the read-out qubit at each iteration step. The algorithm is iterated backwards from the least significant bits of  $\phi$  to the most significant ones. The  $k$ -th iteration is shown in Figure 1.

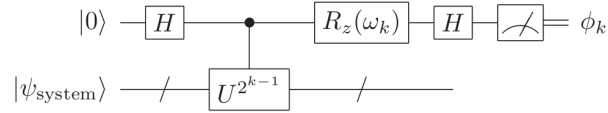


Figure 1: The  $k$ -th iteration of the iterative phase estimation algorithm (IPEA).  $H$  denotes Hadamard gate ( $\pi/2$  rotation) and the feedback angle  $\omega_k$  depends on the previously measured bits (see Eq. 4).

The equivalent of QFT is a single qubit  $z$ -rotation  $R_z$ , whose angle  $\omega_k$  depends on the results of the previously measured bits

$$R_z(\omega_k) = \begin{pmatrix} 1 & 0 \\ 0 & e^{2\pi i \omega_k} \end{pmatrix} \quad (3)$$

$$\omega_k = - \sum_{i=2}^{m-k+1} \frac{\phi_{k+i-1}}{2^i}, \quad (4)$$

followed by a Hadamard gate.

Depending on how the second part of the quantum register is treated in between individual iterations, we distinguish two versions of IPEA<sup>14</sup>. In case of version **A**, it is maintained during all iterations (initialised only once). The biggest advantage of this approach is that one always ends up with one of the eigenstates of  $\hat{U}$ . On the other hand, the quantum coherence is needed for the whole algorithm which makes this version more difficult for an experimental realization. IPEA version **B** is on contrary characterised by reinitialization of the second part of the register at every iteration step. Therefore, the quantum coherence is needed only within each iteration separately.

The (I)PEA algorithm can be exploited for *ab initio* quantum chemical calculations, if we take  $\hat{U}$  in the form<sup>7,11</sup>

$$\hat{U} = e^{i\tau \hat{H}}, \quad (5)$$

where  $\hat{H}$  is the molecular electronic Hamiltonian (up to now, only Born-Oppenheimer Hamiltonians have been considered) and  $\tau$  is a suitable parameter which assures  $\phi$  being in the interval  $(0, 1)$ .

The electronic Hamiltonian can be expressed in the second quantized form as<sup>36</sup>

$$\hat{H} = \sum_{pq} h_{pq} \hat{a}_p^\dagger \hat{a}_q + \frac{1}{2} \sum_{pqrs} V_{pqrs} \hat{a}_p^\dagger \hat{a}_q^\dagger \hat{a}_s \hat{a}_r = \sum_{X=1}^L \hat{h}_X, \quad (6)$$

where  $h_{pq}$  and  $V_{pqrs}$  are one and two-electron integrals in the molecular spin orbital basis and  $\hat{a}_i^\dagger$  and  $\hat{a}_i$  are fermionic creation and annihilation operators. Since these operators in general do not commute, exponential of the Hamiltonian cannot be written as a product of exponentials of individual  $\hat{h}_X$ , but a numerical approximation must be used<sup>2</sup>. The first-order Trotter approximation<sup>37</sup> has the form

$$e^{i\tau\hat{H}} = e^{i\tau\sum_{X=1}^L \hat{h}_X} = \left( \prod_{X=1}^L e^{i\hat{h}_X\tau/N} \right)^N + \mathcal{O}(\tau^2/N). \quad (7)$$

When representing the quantum chemical wave function on a quantum register, the simplest approach (but the least economical one in terms of number of qubits) is so called direct mapping. It directly assigns individual spin orbitals (or in relativistic case Kramers pair bispinors) to qubits, since they can be either occupied or unoccupied (occupation number basis), corresponding to  $|1\rangle$  or  $|0\rangle$  states. Jordan-Wigner transformation (JWT)<sup>38</sup> is then used to express fermionic operators in terms of Pauli  $\sigma$  matrices. JWT has the form

$$\hat{a}_n^\dagger = \left( \bigotimes_{j=1}^{n-1} \sigma_z^j \right) \otimes \sigma_-^n, \quad \hat{a}_n = \left( \bigotimes_{j=1}^{n-1} \sigma_z^j \right) \otimes \sigma_+^n, \quad (8)$$

where  $\sigma_\pm = 1/2(\sigma_x \pm i\sigma_y)$  and the superscript denotes the qubit on which the matrix operates. Alternatively, the Bravyi-Kitaev transformation<sup>39,40</sup> which balances locality of occupation and parity information and reduces the simulation cost from  $\mathcal{O}(n)$  to  $\mathcal{O}(\log n)$  for one fermionic operator when compared to JWT may be used. We would like to note that more compact mappings e.g. from subspace of fixed-electron-number wave functions or spin-adapted wave functions can also be used *efficiently* in connection with quantum sparse simulation algorithms<sup>41</sup>.

Regarding the overall scaling of the qFCI algorithm, Wecker *et al.*<sup>42</sup> found that the computational time for bounded error scales with the number of spin orbitals  $N$  as  $\mathcal{O}(N^9)$  on average and as  $\mathcal{O}(N^{11})$  at worst. Using the Bravyi-Kitaev transformation<sup>39,40</sup> instead of JWT would decrease the scaling to  $\mathcal{O}(N^8 \log N)$  or  $\mathcal{O}(N^{10} \log N)$  respectively. Poulin *et al.*<sup>43</sup> used testing set of real molecules and observed even more feasible scaling of the Trotter-Suzuki time step leading to the overall scaling  $\mathcal{O}(N^{4-5.5})$ . The computational cost bounds can be further improved considering local molecular basis sets<sup>44</sup>.

The qFCI algorithm<sup>11,13</sup> requires an initial guess of the exact eigenstate, whose quality influences the success probability of measuring the desired energy. This can be either a classical approximation [e.g. complete active space (CAS) based wave function<sup>12,14</sup>], an exact state prepared by the adiabatic state preparation method<sup>11,45</sup>, or by the algorithmic cooling method<sup>46</sup>, or also a unitary coupled cluster approximation optimised by the recently presented combined classical-quantum variational approach<sup>26,47</sup>.

In order to increase the overall success probability of (I)PEA, the whole algorithm is repeated and the correct phase  $\phi$  decided from the majority voting. In case of version **B**, individual iterations are independently repeated and correct  $\phi_k$  values decided from the majority voting.

### 3 NOMO method

The nuclear orbital plus molecular orbital (NOMO) theory<sup>28–34</sup> (other authors denote similar theories with different acronyms, e.g. ENMO<sup>48</sup> or NEO<sup>49</sup>) is an extension of MO theory to the non-BOA problem, which employs the idea of a nuclear orbital (NO), as a one-particle orbital of a nucleus. Since electrons and nuclei are treated on equal footing in NOMO framework, it goes beyond the Born-Oppenheimer and adiabatic approximations<sup>50</sup>.

In the NOMO method, Gaussian-type functions are adopted for electronic as well as nuclear basis functions, which leads to difficulties in gauging the total-energy accuracy because of the poor description of translational and rotational motions. For this reason, translation- and rotation-free (TRF) approach has been developed by eliminating the contribution of translation and rotation from the total Hamiltonian<sup>31–34</sup>. The TRF Hamiltonian has the form

$$\begin{aligned}\hat{H}_{\text{TRF}} &= \hat{H} - \hat{T}_{\text{T}} - \hat{T}_{\text{R}} \\ &= \hat{T}_{\text{TRF}}^{\text{n}} + \hat{T}_{\text{TRF}}^{\text{e}} + \hat{V}_{\text{TRF}}^{\text{nn}} + \hat{V}_{\text{TRF}}^{\text{ne}} + \hat{V}_{\text{TRF}}^{\text{ee}}.\end{aligned}\quad (9)$$

The total translational Hamiltonian  $\hat{T}_{\text{T}}$  is simply subtracted, but since molecular rotations and vibrations are coupled, the contribution of rotation cannot be entirely eliminated. The only viable way how to subtract rotation is by Taylor expansion of the rotational Hamiltonian  $\hat{T}_{\text{R}}$  with respect to  $\Delta r_{\mu}$  (as defined in<sup>34</sup>). In our numerical study (see Section 5), this was done just to zeroth order.

The Hamiltonian  $\hat{H}_{\text{TRF}}$  contains one-particle (nucleus:  $\hat{T}_{\text{TRF}}^{\text{n}}$ , electron:  $\hat{T}_{\text{TRF}}^{\text{e}}$ ) and two-particle (nucleus-nucleus:  $\hat{V}_{\text{TRF}}^{\text{nn}}$ , nucleus-electron:  $\hat{V}_{\text{TRF}}^{\text{ne}}$ , electron-electron:  $\hat{V}_{\text{TRF}}^{\text{ee}}$ ) terms and has the same second-quantized form as in Eq. 6. If, for simplicity, we consider now only one kind of nucleus and use big subscripts  $\{P, Q, \dots\}$  for NOs and small  $\{p, q, \dots\}$  for MOs, we can write

$$\begin{aligned}\hat{H}_{\text{TRF}} &= \sum_{pq} h_{pq}^{\text{ee}} \hat{a}_p^{\dagger} \hat{a}_q + \sum_{PQ} h_{PQ}^{\text{nn}} \hat{a}_P^{\dagger} \hat{a}_Q \\ &+ \frac{1}{2} \sum_{pqrs} V_{pqrs}^{\text{ee}} \hat{a}_p^{\dagger} \hat{a}_q^{\dagger} \hat{a}_s \hat{a}_r + \frac{1}{2} \sum_{PQRS} V_{PQRS}^{\text{nn}} \hat{a}_P^{\dagger} \hat{a}_Q^{\dagger} \hat{a}_S \hat{a}_R \\ &+ \sum_{pQrS} V_{pQrS}^{\text{en}} \hat{a}_p^{\dagger} \hat{a}_Q^{\dagger} \hat{a}_S \hat{a}_r.\end{aligned}\quad (10)$$

In principle, the NOMO/FCI theory for a complete configuration space is an exact theory. In practice however, due to the exponential scaling of classical FCI, some approximation has to be adopted. Different kinds of NOMO post-Hartree-Fock methods analogous to those from the conventional Born-Oppenheimer electronic structure theory has been developed, to name a few e.g. NOMO/MP2<sup>30,33</sup>, NOMO/CI<sup>51</sup>, or NOMO/CC<sup>30</sup>. One of the drawbacks of the NOMO theory is a slow convergence of the n-e correlation effect with respect to CI/CC expansion<sup>52–54</sup>. As we are dealing with the NOMO/FCI theory here, which is, as already mentioned, an exact theory, we avoid this problem. For more details about the NOMO methodology and the discussion of its pros and cons, we refer the reader to the original literature<sup>31,52</sup>.

### 4 Quantum NOMO/FCI algorithm

In this section we elaborate how the qFCI algorithm is employed for the NOMO Hamiltonian (10). Despite restricting ourselves to distinguishable nuclei in the proof-of-principle numerical simula-

tions, the presentation in this section is intentionally kept as general as possible, i.e. considering several types of fermionic and/or bosonic nuclei.

The NOMO Hamiltonian (10) can be cast to the general form (6), if the indices  $p, q, r, s$  are allowed to run over nuclei spin orbitals as well, i.e.  $h_{pq}$  and  $V_{pqrs}$  stands for one and two-particle integrals over molecular and/or nuclear spin orbitals. For this we define the following ordering of the electronic and nuclear spin orbitals. Let us consider a general system consisting of  $K$  kinds of different nuclei, where we have  $N_0$  molecular spin orbitals for  $n_0$  electrons,  $N_1$  nuclear spin orbitals for  $n_1$  nuclei of the 1st kind, etc., up to  $N_K$  nuclear spin orbitals for  $n_K$  nuclei of the  $K$ -th kind. Say that  $K_{\text{ferm}}$  kinds correspond to fermionic nuclei and the rest to bosonic ones.

Therefore  $p, q, r, s \in \{1, 2, \dots, N_T\}$ , where  $N_T$  is the total number of spin orbitals

$$N_T = \sum_{k=0}^K N_k. \quad (11)$$

The operator  $\hat{a}_p^\dagger$  in (6) denotes the creation operator for  $p$ -th spin orbital [creating either electron (for  $p \leq N_0$ ) or nucleus (for  $p > N_0$ )] and  $\hat{a}_q$  is the annihilation operator.

The  $k$ -th kind nuclear spin orbital indices belong to the set  $S_k$

$$S_k = \{I_k, I_k + 1, \dots, I_k + N_k - 1\}, \quad (12)$$

where  $I_k$  is the  $k$ -th nuclei starting index

$$I_k = \sum_{i=0}^{k-1} N_i + 1. \quad (13)$$

All creation and annihilation operators commute with both creation and annihilation operators for different particles

$$\begin{aligned} [\hat{a}_p^\dagger, \hat{a}_q^\dagger] &= [\hat{a}_p^\dagger, \hat{a}_q] = [\hat{a}_p, \hat{a}_q] = 0, \\ \text{if } p \in S_k, q \in S_l \text{ and } k \neq l. \end{aligned} \quad (14)$$

If particles of  $k$ -th kind are fermionic, the usual anticommutation relation holds

$$\begin{aligned} \{\hat{a}_p^\dagger, \hat{a}_q^\dagger\} &= \{\hat{a}_p, \hat{a}_q\} = 0, \quad \{\hat{a}_p^\dagger, \hat{a}_q\} = \delta_{pq}, \\ \text{if } p, q \in S_k \text{ and fermions,} \end{aligned} \quad (15)$$

while bosonic nuclei must obey the commutation relations

$$\begin{aligned} [\hat{a}_p^\dagger, \hat{a}_q^\dagger] &= [\hat{a}_p, \hat{a}_q] = 0, \quad [\hat{a}_p^\dagger, \hat{a}_q] = \delta_{pq}, \\ \text{if } p, q \in S_k \text{ and bosons.} \end{aligned} \quad (16)$$

Distinguishable identical nuclei can be considered as separate classes of different nuclei, each class consisting of a single nucleus, so that the relations (14) apply.

The mapping between (anti)symmetrized products of spin orbitals of our general system and states of a quantum register can be constructed in the following way. Let us order the nuclei classes so that fermionic nuclei ( $k \leq K_{\text{ferm}}$ ) precedes the bosonic ones ( $k > K_{\text{ferm}}$ ) and discuss the mapping for different particle types separately.

#### 4.0.1 Fermions

For fermions of  $k$ -th kind ( $p \in S_k$ ), the standard Jordan-Wigner mapping (8) can be used, which in our index convention can be expressed as

$$\hat{a}_p^\dagger = \left( \bigotimes_{\substack{i \in S_k \wedge \\ i < p}} \sigma_z^i \right) \otimes \sigma_-^p, \quad (17)$$

$$\hat{a}_p = \left( \bigotimes_{\substack{i \in S_k \wedge \\ i < p}} \sigma_z^i \right) \otimes \sigma_+^p. \quad (18)$$

When individual  $\exp(i\hat{h}_X\tau/N)$  (see Eq. 7) terms are implemented, this approach leads to the computational cost  $\mathcal{O}(N_k^5)$ . Alternatively, the more economic Bravyi-Kitaev transformation<sup>39,40</sup> [ $\mathcal{O}(N_k^4 \log N_k)$ ] can be employed.

#### 4.0.2 Bosons

In contrast to fermions, more than one qubit is needed to store an occupation number of a bosonic spin orbital. When considering bosonic particles of  $k$ -th kind, the occupation number  $f(p)$  of the spin orbital  $p$  can acquire values from 0 to  $n_k$ . The so called direct boson mapping<sup>5</sup> uses  $n_k + 1$  qubits to store this occupation number in the following way

$$|f(p)\rangle = \left( \bigotimes_{i=0}^{f(p)-1} |0\rangle_i \right) \otimes |1\rangle_{f(p)} \otimes \left( \bigotimes_{i=f(p)+1}^{n_k} |0\rangle_i \right). \quad (19)$$

For clarity, we take into account only the part of a quantum register that corresponds to  $p$ -th spin orbital (in bosonic case one creation or annihilation operator does not act on qubits corresponding to different spin orbitals).

From (16) follows the action of creation and annihilation operators

$$\hat{a}_p^\dagger |f(p)\rangle = \sqrt{f(p)+1} |f(p)+1\rangle, \quad (20)$$

$$\hat{a}_p |f(p)\rangle = \sqrt{f(p)} |f(p)-1\rangle, \quad (21)$$

$$\hat{a}_p |0\rangle = 0. \quad (22)$$

As the maximum occupation  $f(p)$  is the number of particles  $n_k$ , one more condition has to be introduced

$$\hat{a}_p^\dagger |n_k\rangle = 0. \quad (23)$$

In analogy to Eqs. (17) and (18), Somma *et al.*<sup>5</sup> proposed the direct boson mapping of the form

$$\hat{a}_p^\dagger = \sum_{j=0}^{n_k-1} \sqrt{j+1} (\sigma_+^j \otimes \sigma_-^{j+1}), \quad (24)$$

$$\hat{a}_p = \sum_{j=0}^{n_k-1} \sqrt{j+1} (\sigma_-^j \otimes \sigma_+^{j+1}). \quad (25)$$

Following their complexity analysis, we can express the overall computational cost of a single Trotter step of the general system as

$$\begin{aligned}
& \mathcal{O}\left(\sum_{0 \leq k \leq l \leq K_{\text{ferm}}} N_k^2 N_l^2 \log(N_k N_l)\right) + \\
& + \mathcal{O}\left(\sum_{K_{\text{ferm}} < k \leq l \leq K} n_k^2 n_l^2 N_k N_l^2\right) + \\
& + \mathcal{O}\left(\sum_{\substack{0 \leq k \leq K_{\text{ferm}} \\ K_{\text{ferm}} < l \leq K}} n_l^2 \log(N_k) N_l N_k^2\right), \tag{26}
\end{aligned}$$

where individual terms correspond to contributions from fermion-fermion, boson-boson and fermion-boson interactions, respectively, and  $N_k \leq N_l$  for each  $K_{\text{ferm}} + 1 \leq k < l$  is supposed for simplicity. The Bravyi-Kitaev transformation is considered for fermions in (26), as well as in the following formulae (30) and (32).

In contrast to the direct boson mapping, we propose the compact boson mapping which uses only  $\lceil \log_2(n_k + 1) \rceil$  qubits to represent the binary expansion of  $f(p)$ , as shown below (the least significant bit is written leftmost)

$$\begin{aligned}
|f(p)=0\rangle & \mapsto |0\rangle|0\rangle|0\rangle\ldots|0\rangle, \\
|f(p)=1\rangle & \mapsto |1\rangle|0\rangle|0\rangle\ldots|0\rangle, \\
|f(p)=2\rangle & \mapsto |0\rangle|1\rangle|0\rangle\ldots|0\rangle, \\
|f(p)=3\rangle & \mapsto |1\rangle|1\rangle|0\rangle\ldots|0\rangle, \text{ etc.} \tag{27}
\end{aligned}$$

The representation of creation and annihilation operators for  $p$ -th spin orbital is defined implicitly by relations (20)-(23) and we can express them semi-formally by the formulae

$$\hat{a}_p^\dagger = \sum_{j=0}^{n_k-1} \sqrt{j+1} |f(p)=j+1\rangle \langle f(p)=j|, \tag{28}$$

$$\hat{a}_p = \sum_{j=0}^{n_k-1} \sqrt{j+1} |f(p)=j\rangle \langle f(p)=j+1|. \tag{29}$$

Rather than using formulae (28) and (29) explicitly, circuit representation of appropriate combinations of the bosonic creation and annihilation operators occurring in (10) were investigated. In the Appendix we show that this approach leads to the overall computational cost of a single Trotter step



$$\begin{aligned}
& \mathcal{O}\left(\sum_{0 \leq k \leq l \leq K_{\text{ferm}}} N_k^2 N_l^2 \log(N_k N_l)\right) + \\
& \mathcal{O}\left(\sum_{K_{\text{ferm}} < k \leq l \leq K} N_g(n_k, n_l) N_k N_l^2\right) + \\
& + \mathcal{O}\left(\sum_{\substack{0 \leq k \leq K_{\text{ferm}} \\ K_{\text{ferm}} < l \leq K}} N_g(1, n_l) \log(N_k) N_l N_k^2\right),
\end{aligned} \tag{30}$$

where

$$\begin{aligned}
N_g(n, m) = & -\frac{1}{15}y + \frac{1}{3}xy(x+y) + \\
& + \frac{2}{3}x^2y^3 - \frac{1}{3}xy^4 + \frac{1}{15}y^5,
\end{aligned} \tag{31}$$

$x = \max(n, m) + 1$ ,  $y = \min(n, m) + 1$ . The derivation of (30) (See Appendix) took into account that bosonic terms with non-overlapping sets of indices can be processed simultaneously.

In the simplified case where  $n_k = n$  for each  $k > K_{\text{ferm}}$   $N_g(n, n) = \mathcal{O}(n^5)$  and  $N_g(1, n) = \mathcal{O}(n^2)$  and the single Trotter step overall computational cost is

$$\begin{aligned}
& \mathcal{O}\left(\sum_{0 \leq k \leq l \leq K_{\text{ferm}}} N_k^2 N_l^2 \log(N_k N_l)\right) + \\
& + \mathcal{O}\left(\sum_{K_{\text{ferm}} < k \leq l \leq K} n^5 N_k N_l^2\right) + \\
& + \mathcal{O}\left(\sum_{\substack{0 \leq k \leq K_{\text{ferm}} \\ K_{\text{ferm}} < l \leq K}} n^2 \log(N_k) N_l N_k^2\right).
\end{aligned} \tag{32}$$

#### 4.0.3 Distinguishable particles

Distinguishable particles can be distributed to separate classes each with  $n_k = 1$  and occupation numbers  $f(p) \in \{0; 1\}$  with  $p \in S_k$  can be stored using one qubit per spin orbital for each of the particles. The creation and annihilation operators can then be represented as

$$\hat{a}_p^\dagger = \sigma_-^p, \tag{33}$$

$$\hat{a}_p = \sigma_+^p \tag{34}$$

and we can use either (26) or (32), which are in fact equivalent in this case as  $n_k = 1$ .

The equations (26) and (32) demonstrate that the qFCI algorithm can be *efficient* also for systems with bosonic and/or distinguishable particles. In case of the compact boson mapping, the smaller number of qubits needed to represent a state of a molecule (as compared with the direct boson mapping) is paid by worse computational cost in terms of the number of two-qubit gates

needed for a computation. For the first, few-qubit quantum computers, the compact boson mapping should be important, however for larger scale quantum computers, the direct boson mapping is of much greater importance.

We would like to note that presented mappings are not restricted to (I)PEA algorithm only. They, in fact, can be also used in connection with other methods that were developed to reduce qubit and coherence time requirements<sup>21,23,26,55</sup>, i.e. to adapt the procedure for a present-day or near-future quantum technology.

## 5 Application to H<sub>2</sub> and HT molecules

### 5.1 Computational details

For the proof-of-principle classical simulations, we have chosen the simplest molecular examples, namely the two isotopomers of the hydrogen molecule (H<sub>2</sub>, HT). For MOs, we employed the cc-pVTZ basis set, while NOs were expanded in a basis of one *s*, one *p*, and one *d* non-contracted Gaussians centred on each hydrogen atom with five even-tempered exponents from 9.081045 to 908.104502 for H and from 27.18608 to 2718.608 for T isotope (total 50 nuclear basis functions for each hydrogen atom). The internuclear distance was fixed to  $R = 0.750746$  Å.

The nuclei were for simplicity treated as distinguishable which is the usual procedure that can be justified by the fact that exchange interaction between nuclei is negligibly small.

We worked solely with a compact mapping from subspace of wave functions with zero *z*-component of total electron and nuclear spins and the exponential of a Hamiltonian was simulated as an *n*-qubit gate (similarly as in Refs.<sup>11,12,14,15</sup>). We simulated  $m = 17$  iterations of both IPEA **A** and **B** with input parameters (see Ref.<sup>14</sup>)  $E_{\min} = -1.20$  a.u. and  $E_{\max} = -1.00$  a.u.

The ground state of both H<sub>2</sub> and HT is dominated by  $1\sigma_g^2 1\sigma_{n1} 1\sigma_{n2}$  configuration, while the excited state  $\nu = 1, J = 0$  was identified as a state dominated by  $1\sigma_g^2 2\sigma_{n1} 2\sigma_{n2}$  configuration. Between all states in  $\pm 50\%$  interval around the experimental transition energy, only this state is non-degenerate and symmetric with respect to the exchange of the nuclear coordinates (and therefore has even rotation number *J* and is a nuclear singlet).

The initial guesses of both states were single determinants (ground state:  $1\sigma_g^2 1\sigma_{n1} 1\sigma_{n2}$ , excited state:  $1\sigma_g^2 2\sigma_{n1} 2\sigma_{n2}$ ).

However, we must note that for larger polyatomic molecules the identification of several rotationless vibrational excited states and the choice of sufficiently accurate initial guesses of eigenvectors for IPEA might be much more complicated than it was for the hydrogen molecule.

### 5.2 Results

In Table 1, we show energies and IPEA (**A**) success probabilities for the ground and excited states of H<sub>2</sub>, while Table 2 presents minimal number of repetitions of IPEA **A** and IPEA **B** needed to achieve a given success probability (0.99, 0.999 999). Tables 3 and 4 give corresponding information for the HT molecule.

The exponential increase of success probabilities *p* with the number of repetitions *r* (as supposed from the Chernoff bounds<sup>66</sup>) is demonstrated in Fig. 2 (for the case of basis consisting of  $N = 6$  molecular and  $M = 10$  nuclear orbitals) and Fig. 3 ( $N = 9, M = 23$ ) by roughly asymptotically linear curves of quantity  $f(r) = -\log(1 - p)$  as a function of *r*.

For almost all data points, the success probabilities for IPEA **A** are higher than corresponding success probabilities for IPEA **B** and the slope of  $f(r)$  curve in asymptotic region is subsequently also higher for IPEA **A** than for IPEA **B**. In most cases, we can also see higher values and slopes

$N$	$M$	MOs	NOs	$E_{\text{gs}}$ a.u.	$E_{\text{es}}$ a.u.	$\Delta E$ $\text{cm}^{-1}$	$\delta\omega$	$S_{\text{gs}}$	$S_{\text{es}}$	$p_{\text{A,gs}}$	$p_{\text{A,es}}$
1	4	$\sigma_{\text{g}}$	$2\sigma\pi$	-1.104049	-1.080972	5064.8	21.7	0.9985	0.9164	0.8217	0.8743
2	6	$\sigma_{\text{g}}\sigma_{\text{u}}$	$2\sigma\pi\delta$	-1.105483	-1.082857	4965.7	19.3	0.9973	0.6737	0.9645	0.5760
3	8	$2\sigma_{\text{g}}\sigma_{\text{u}}$	$2\sigma 2\pi\delta$	-1.108131	-1.085068	5061.7	21.6	0.9880	0.7784	0.8073	0.7780
4	10	$2\sigma_{\text{g}}2\sigma_{\text{u}}$	$4\sigma 2\pi\delta$	-1.119317	-1.096120	5091.1	22.3	0.9759	0.8344	0.8769	0.6779
6	10	$2\sigma_{\text{g}}2\sigma_{\text{u}}\pi_{\text{u}}$		-1.127425	-1.107187	4441.8	6.7	0.9583	0.9385	0.9419	0.8454
6	15		$5\sigma 3\pi 2\delta$	-1.127443	-1.107373	4404.8	5.9	0.9575	0.9282	0.9329	0.9102
6	23		$7\sigma 5\pi 3\delta$	-1.127612	-1.108051	4293.3	3.2	0.9571	0.9135	0.9565	0.9095
7	18	$3\sigma_{\text{g}}2\sigma_{\text{u}}\pi_{\text{u}}$	$6\sigma 3\pi 3\delta$	-1.129852	-1.109358	4497.9	8.1	0.9404	0.9041	0.8113	0.8056
7	23		$7\sigma 5\pi 3\delta$	-1.129917	-1.110242	4318.0	3.8	0.9464	0.8900	0.9059	0.7301
9	10	$3\sigma_{\text{g}}2\sigma_{\text{u}}\pi_{\text{u}}\pi_{\text{g}}$	$4\sigma 2\pi\delta$	-1.130100	-1.109888	4436.0	6.6	0.9419	0.9053	0.7718	0.7387
9	18		$6\sigma 3\pi 3\delta$	-1.130285	-1.110317	4382.5	5.3	0.9334	0.8779	0.7971	0.8735
9	20		$6\sigma 4\pi 3\delta$	-1.130293	-1.110419	4361.9	4.8	0.9342	0.8880	0.9316	0.8455
9	23		$7\sigma 5\pi 3\delta$	-1.130346	-1.111238	4193.7	0.8	0.9398	0.8600	0.8376	0.7394
		Theory non-rel. <sup>1</sup>		-1.164025	-1.145065	4161.2					
		Theory rel. <sup>2</sup>		-1.164033	-1.145073	4161.2					
		Experiment <sup>3</sup>		-1.164033	-1.145073	4161.2					

Table 1: Ground ( $E_{\text{gs}}$ ) and excited state ( $E_{\text{es}}$ ,  $\nu = 1$ ,  $J = 0$ ) NOMO-TRF/FCI energies and IPEA (**A**) success probabilities ( $p_{\text{A,gs}}$ ,  $p_{\text{A,es}}$ ) for the  $\text{H}_2$  molecule in the basis consisting of  $N$  molecular orbitals and  $M$  nuclear orbitals.  $\Delta E$  denotes transitional energy,  $\delta\omega = 100(\Delta E - \Delta E_{\text{exp}})/\Delta E_{\text{exp}}$ ,  $S_{\text{gs}}$  and  $S_{\text{es}}$  denote square of absolute value of the overlaps between NOMO-TRF/FCI eigenvectors and their initial guesses.

of curves corresponding to ground state when compared to the excited state. This correlates with the fact that excited state NOMO-TRF/FCI eigenvector has smaller overlap with its initial guess than the ground state. In other words, the excited state has stronger multireference character.

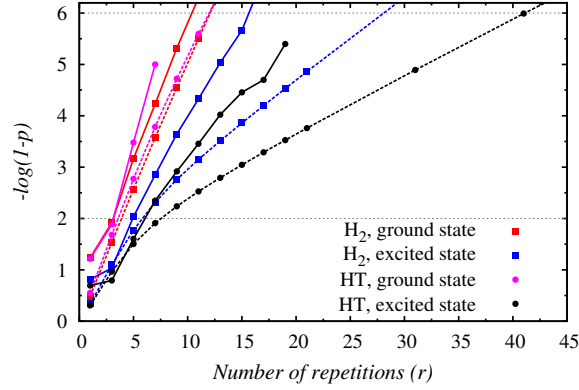


Figure 2: NOMO-TRF/qFCI success probabilities  $p$  (IPEA **A** - solid line, IPEA **B** - dashed line) for both  $\text{H}_2$  and HT molecules in the basis consisting of  $N = 6$  molecular and  $M = 10$  nuclear orbitals as a function of the number of repetitions ( $r$ ).

### 5.3 Discussion

Results presented in the previous section indicate that for all choices of the FCI active space [defined by the number of molecular ( $N$ ) and nuclear ( $M$ ) orbitals], single determinant initial guesses give

$N$	$M$	MOs	NOs	$N_{B,gs,2}$	$N_{A,gs,2}$	$N_{B,gs,6}$	$N_{A,gs,6}$	$N_{B,es,2}$	$N_{A,es,2}$	$N_{B,es,6}$	$N_{A,es,6}$
1	4	$\sigma_g$	$2\sigma\pi$	7	7	37	29	7	7	21	23
2	6	$\sigma_g\sigma_u$	$2\sigma\pi\delta$	3	3	11	7	39	63	131	253
3	8	$2\sigma_g\sigma_u$	$2\sigma 2\pi\delta$	9	7	37	29	13	9	45	35
4	10	$2\sigma_g 2\sigma_u$	$4\sigma 2\pi\delta$	5	5	25	15	11	13	41	39
6	10	$2\sigma_g 2\sigma_u \pi_u$		5	5	13	11	7	5	29	17
6	15		$5\sigma 3\pi 2\delta$	5	5	13	13	5	5	17	13
6	23		$7\sigma 5\pi 3\delta$	5	3	13	11	7	5	19	15
7	18	$3\sigma_g 2\sigma_u \pi_u$	$6\sigma 3\pi 3\delta$	7	7	37	23	9	7	37	21
7	23		$7\sigma 5\pi 3\delta$	5	5	15	15	11	11	43	35
9	10	$3\sigma_g 2\sigma_u \pi_u \pi_g$	$4\sigma 2\pi\delta$	9	9	39	31	11	9	55	33
9	18		$6\sigma 3\pi 3\delta$	9	9	47	27	7	5	23	13
9	20		$6\sigma 4\pi 3\delta$	5	5	17	11	7	5	23	15
9	23		$7\sigma 5\pi 3\delta$	7	7	27	19	11	9	43	27

Table 2: Minimal number of repetitions for IPEA **B** to achieve success probability at least  $p = 0.99$  ( $N_{B,y,2}$ ) or at least  $p = 0.999\ 999$  ( $N_{B,y,6}$ ) and the same quantities for IPEA **A** ( $N_{A,y,2}$ ,  $N_{A,y,6}$ ), where  $y \in \{\text{gs(ground state), es(excited state)}\}$ . All data corresponds to  $H_2$  molecule.

$N$	$M$	MOs	NOs	$E_{gs}$ a.u.	$E_{es}$ a.u.	$\Delta E$ $\text{cm}^{-1}$	$\delta\omega$	$S_{gs}$	$S_{es}$	$p_{A,gs}$	$p_{A,es}$
1	4	$\sigma_g$	$2\sigma\pi$	-1.109233	-1.091291	3937.9	14.6	0.9989	0.9171	0.9968	0.8171
2	6	$\sigma_g\sigma_u$	$2\sigma\pi\delta$	-1.11064	-1.092828	3909.1	13.8	0.9977	0.8853	0.9769	0.8736
3	7	$2\sigma_g\sigma_u$	$2\sigma 2\pi\delta$	-1.112491	-1.094738	3896.2	13.4	0.9946	0.8903	0.9784	0.7993
4	10	$2\sigma_g 2\sigma_u$	$4\sigma 2\pi\delta$	-1.124135	-1.106038	3971.8	15.6	0.9766	0.8359	0.9475	0.782
6	10	$2\sigma_g 2\sigma_u \pi_u$		-1.13208	-1.116166	3492.7	1.7	0.9579	0.9294	0.9393	0.7986
6	15		$5\sigma 3\pi 2\delta$	-1.132094	-1.11623	3481.8	1.3	0.9571	0.9175	0.9513	0.834
6	23		$7\sigma 5\pi 3\delta$	-1.132224	-1.116776	3390.5	-1.3	0.957	0.9016	0.7987	0.8004
7	18	$3\sigma_g 2\sigma_u \pi_u$	$6\sigma 3\pi 3\delta$	-1.134359	-1.118117	3564.7	3.8	0.9369	0.8881	0.7712	0.8433
7	23		$7\sigma 5\pi 3\delta$	-1.134412	-1.118831	3419.7	-0.5	0.9438	0.88	0.9396	0.8304
9	10	$3\sigma_g 2\sigma_u \pi_u \pi_g$	$4\sigma 2\pi\delta$	-1.134605	-1.118688	3493.3	1.7	0.9394	0.888	0.8261	0.7207
9	18		$6\sigma 3\pi 3\delta$	-1.134755	-1.118924	3474.5	1.1	0.9297	0.8344	0.8579	0.7891
9	20		$6\sigma 4\pi 3\delta$	-1.134757	-1.119021	3453.7	0.5	0.9303	0.8501	0.7582	0.7359
9	23		$7\sigma 5\pi 3\delta$	-1.134803	-1.119656	3324.4	-3.2	0.937	0.8321	0.7712	0.7804
		Theory non-rel. <sup>4</sup>		-1.166002							
		Theory rel. <sup>5</sup>		-1.166007	-1.150354	3435.5					
		Experiment <sup>6</sup>				3434.8					

Table 3: Ground ( $E_{gs}$ ) and excited state ( $E_{es}$ ,  $\nu = 1$ ,  $J = 0$ ) NOMO-TRF/FCI energies and IPEA (**A**) success probabilities ( $p_{A,gs}$ ,  $p_{A,es}$ ) for the  $H_2$  molecule in the basis consisting of  $N$  molecular orbitals and  $M$  nuclear orbitals.  $\Delta E$  denotes transitional energy,  $\delta\omega = 100(\Delta E - \Delta E_{\text{exp}})/\Delta E_{\text{exp}}$ ,  $S_{gs}$  and  $S_{es}$  denote square of absolute value of the overlaps between NOMO-TRF/FCI eigenvectors and their initial guesses.

$N$	$M$	MOs	NOs	$N_{B,gs,2}$	$N_{A,gs,2}$	$N_{B,gs,6}$	$N_{A,gs,6}$	$N_{B,es,2}$	$N_{A,es,2}$	$N_{B,es,6}$	$N_{A,es,6}$
1	4	$\sigma_g$	$2\sigma\pi$	3	1	5	5	7	7	29	21
2	6	$\sigma_g\sigma_u$	$2\sigma\pi\delta$	3	3	9	7	7	7	21	17
3	7	$2\sigma_g\sigma_u$	$2\sigma 2\pi\delta$	3	3	9	7	9	7	31	21
4	10	$2\sigma_g 2\sigma_u$	$4\sigma 2\pi\delta$	3	5	13	9	11	7	35	23
6	10	$2\sigma_g 2\sigma_u \pi_u$		5	5	13	9	9	7	43	21
6	15		$5\sigma 3\pi 2\delta$	5	5	13	11	7	7	29	19
6	23		$7\sigma 5\pi 3\delta$	9	7	41	25	9	7	33	19
7	18	$3\sigma_g 2\sigma_u \pi_u$	$6\sigma 3\pi 3\delta$	9	9	41	31	7	5	19	15
7	23		$7\sigma 5\pi 3\delta$	5	5	15	11	7	5	25	15
9	10	$3\sigma_g 2\sigma_u \pi_u \pi_g$	$4\sigma 2\pi\delta$	7	7	31	21	11	11	51	35
9	18		$6\sigma 3\pi 3\delta$	7	5	25	17	11	7	29	21
9	20		$6\sigma 4\pi 3\delta$	11	9	39	33	11	9	41	25
9	23		$7\sigma 5\pi 3\delta$	9	9	41	31	11	7	29	19

Table 4: Minimal number of repetitions for IPEA **B** to achieve success probability at least  $p = 0.99$  ( $N_{B,y,2}$ ) or at least  $p = 0.999\ 999$  ( $N_{B,y,6}$ ) and the same quantities for IPEA **A** ( $N_{A,y,2}$ ,  $N_{A,y,6}$ ), where  $y \in \{\text{gs(ground state), es(excited state)}\}$ . All data corresponds to HT molecule.

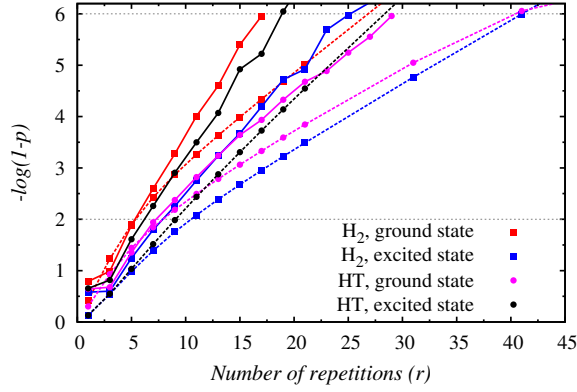


Figure 3: NOMO-TRF/qFCI success probabilities  $p$  (IPEA **A** - solid line, IPEA **B** - dashed line) for both  $H_2$  and HT molecules in the basis consisting of  $N = 9$  molecular and  $M = 23$  nuclear orbitals as a function of the number of repetitions ( $r$ ).

sufficiently high success probabilities to be amplified by repetitions ( $p > 0.5$ ). In most cases, success probabilities are higher than 0.75. The only exception when the success probability is lower than 0.6 is the case of the  $H_2$  excited state and  $N = 2$ ,  $M = 6$ . This choice of the FCI active space is apparently too small to properly describe the transitional energy anyway.

Apart from the  $N = 2$ ,  $M = 6$  active space, results in Tables 2 and 4 indicate that at most around 10 repetitions are sufficient to amplify the success probabilities to 0.99, and at most 55 repetitions for amplification to 0.999999.

For almost all data points, the success probabilities  $p$  for IPEA **A** are higher than corresponding success probabilities for IPEA **B** and subsequently slopes of  $f(r) = -\log(1-p)$  curves in asymptotic region are also higher. This could be easily expected as in case of IPEA **B**, no collapsing of the system and improving the overlap between the actual state of the quantum register and the exact wave function occurs during iterations which is in contrast to IPEA **A**.

In most cases, we can also note higher values and slopes of curves corresponding to ground state when compared to the excited state. The only exception is the case of the largest active space

used ( $N = 9$ ,  $M = 23$ ) for the HT molecule (Fig. 3). Lower success probabilities for the excited state correlates with the excited state NOMO-TRF/FCI eigenvector having smaller overlap with its initial guess than the ground state (stronger multireference character of the excited state)

In the exceptional case ( $N = 9$ ,  $M = 23$  for HT), the overlap for the ground state  $S_{\text{gs}}$  is higher than the overlap for the excited state  $S_{\text{es}}$ , but due to the higher phase reminder  $\delta$  (see eqs. 8 and 9 in<sup>14</sup>) for the ground state, the success probability of non-repeated ( $r = 1$ ) IPEA **A** is slightly higher for the excited state than for the ground state. The phase reminder has the same effect for repeated IPEA success probabilities in both IPEA **A** and IPEA **B** cases.

## 6 Conclusions

In this paper we presented an efficient quantum algorithm for molecular energy computation beyond the Born-Oppenheimer approximation. Our approach is based on the quantum full configuration interaction method and treats electrons and nuclei on an equal footing, using the nuclear orbital plus molecular orbital (NOMO) method. We have presented details of the algorithm and demonstrated its performance by simulations on a classical computer. For these simulations we have employed relatively small one-particle basis sets and used the compact mapping to keep the number of required qubits manageable.

Two isotopomers of the hydrogen molecule ( $\text{H}_2$ , HT) were chosen as representative examples and calculations of the lowest rotationless vibrational transition energies were simulated. For both isotopomers in their ground as well as excited state we have verified that the single-determinant initial guess yields high enough success probability to be amplified by repetitions, for both **A** and **B** version of IPEA. At most 10 repetitions were sufficient to amplify the success probability to 0.99 and at most 55 repetitions were necessary to achieve 0.999999 success probability. As expected, for most data points the success probability of IPEA **A** was higher than corresponding IPEA **B**, due to the improvement of system wave function overlap due to the measurement in the IPEA **A** procedure. In most cases, the excited state required more repetitions than the ground state, which is in agreement with our previous experience on electronic-only calculations<sup>14</sup>. To conclude, the qFCI approach has been shown to be viable also for simultaneous treatment of electrons and nuclei beyond the Born-Oppenheimer approximation.

## Appendix

For derivation of the scaling of the compact boson mapping introduced in Section 4, let us consider the Hamiltonian parameterised by real-valued integrals  $V_{pqrs} = V_{rspq}$  and the most demanding 4-index term of a single Trotter step

$$\exp\left(i\tau V_{pqrs}(\hat{a}_p^\dagger \hat{a}_q^\dagger \hat{a}_s \hat{a}_r + \hat{a}_r^\dagger \hat{a}_s^\dagger \hat{a}_q \hat{a}_p)\right), \quad (35)$$

with  $p$ ,  $q$ ,  $r$ , and  $s$  mutually different. We use the lemma

$$\exp(i\tau\Phi\hat{V}) = \exp(i\tau\Phi\hat{U}\hat{D}\hat{U}^\dagger) = \hat{U} \exp(i\tau\Phi\hat{D})\hat{U}^\dagger, \quad (36)$$

where  $\tau$  and  $\Phi \equiv V_{pqrs}$  are real numbers,  $\hat{V}$  is a hermitian operator and  $\hat{D} = \hat{U}^\dagger \hat{V} \hat{U}$  is its diagonal form. It is thus sufficient to find eigenvectors and eigenvalues of the operator  $\hat{V} = \hat{a}_p^\dagger \hat{a}_q^\dagger \hat{a}_s \hat{a}_r + \hat{a}_r^\dagger \hat{a}_s^\dagger \hat{a}_q \hat{a}_p$  on a Hilbert space corresponding to the quantum register storing occupation numbers for spinorbitals  $p$ ,  $q$ ,  $r$  and  $s$ . This space is a direct product of two  $f_{\text{max}}(p) + 1 = f_{\text{max}}(r) + 1$

dimensional and two  $f_{\max}(q) + 1 = f_{\max}(s) + 1$  dimensional spaces. In the basis characterized by boson occupation numbers the operator  $\hat{V}$  has a block-diagonal structure, since

$$\begin{aligned} \hat{V}|f_p, f_q, f_r, f_s\rangle = \\ = \sqrt{(f_p + 1)(f_q + 1)f_r f_s}|f_p + 1, f_q + 1, f_r - 1, f_s - 1\rangle + \\ \sqrt{f_p f_q(f_r + 1)(f_s + 1)}|f_p - 1, f_q - 1, f_r + 1, f_s + 1\rangle. \end{aligned} \quad (37)$$

In the simplest case of  $f_{\max}(p) = f_{\max}(q) = n$  there are  $12(n+1-d)+2-\delta_{n+1,d}$   $d$ -dimensional blocks ( $d = 1, 2, \dots, n+1$ ). In general, the number of diagonal  $d$ -dimensional blocks ( $d = 1, 2, \dots, \min(n_1, n_2)+1$ ) denoted here  $p_d$ , equals (see the Supplementary Information, Chapter 2.1.)

$$\begin{aligned} p_d = -\delta_{z,0}(|n_1 - n_2| - 1)^2 + \\ + 2(|n_1 - n_2|^2 + 1) + 6z(|n_1 - n_2| + z) \end{aligned} \quad (38)$$

where  $z = \min(n_1, n_2) + 1 - d$  and  $n_1 = f_{\max}(p) = f_{\max}(r)$  and  $n_2 = f_{\max}(q) = f_{\max}(s)$ . Decomposition of the matrix representation of  $\hat{V}$  ( $V$ ) and then subsequently  $U$  into blocks leads to a decomposition of  $\hat{U}$  from lemma (36) to a direct sum of unitary operators  $\hat{U}_i$  acting on each block

$$\hat{U} = \bigoplus_{i=0}^K \hat{U}_i. \quad (39)$$

Let us define

$$M_{S,s} = \sum_{d=1}^{\min(n_1, n_2)+1} d^s p_d, \quad (40)$$

where  $s$  is an auxiliary non-negative integer.  $M_{S,s}$  has a different meaning depending on  $s$  value.

For  $s = 0$ ,  $M_{S,s}$  equals the total number of subspaces  $K = M_{S,0} = n_1 n_2 (n_1 + n_2 + 1)$  in the decomposition (39).

The dimension of the quantum register space where operator (35) acts is  $M_{S,1} = (n_1 + 1)^2 (n_2 + 1)^2$ .  $M_{S,1}$  is in fact the minimal possible size of the quantum register for representing operator (35). In the case of qubits, the quantum register dimension will be  $2^{2\lceil \log_2(n_1+1) \rceil + 2\lceil \log_2(n_2+1) \rceil} \geq (n_1 + 1)^2 (n_2 + 1)^2 = M_{S,1}$ . Usage of qu- $d$ -its for well chosen  $d$ 's may decrease the “excess” dimensions usually padded by unit operator blocks and the number  $C(n_1, n_2)$  of classical precomputing operations needed for the diagonalization of matrix representation (35).

For  $s = 2$ ,  $M_{S,2} = N_g(n_1, n_2)$  describes the computational complexity as will be shown in the end of this section.

The computational cost of classical precomputing operations scales as  $C(n_1, n_2) = M_{S,3}$ .

Based on the above approach, the exponential (35) can be decomposed into blocks,

$$\exp(i\tau\Phi\hat{V}) = \bigoplus_{i=0}^K \hat{A}_i, \quad (41)$$

$$\hat{A}_i = \hat{U}_i \exp(i\tau\Phi\hat{D}_i) \hat{U}_i^\dagger, \quad (42)$$

where  $\hat{D}_i$  is a diagonal gate with only  $d_i$  non-zero elements. Gates  $\hat{A}_i$  in the circuit correspond to the product (42) and are further described in Fig. 5. Before and after the sequence of  $\hat{A}_i$  gates is applied, the transformation

$$\begin{aligned} |f_p, f_q, f_r, f_s\rangle &\mapsto |\Sigma_1, \Delta_1, \Delta_2, \Sigma_2\rangle \mapsto \\ &\mapsto |\Delta, \Delta_1, \Delta_2, \Sigma\rangle, \end{aligned} \quad (43)$$

and its inverse have to be applied as shown in Fig. 4 (The transformation (43) is realized by the subcircuit in the dashed box (Fig. 4, the gate  $\hat{W}$ ).

The non-negative integers  $f_p, f_q, f_r$  and  $f_s$  are occupation numbers, their upper-bounds are  $f_p, f_r \leq n_1$  and  $f_q, f_s \leq n_2$  (and corresponding register sizes in qubits  $Q_1 = \lceil \log_2(n_1 + 1) \rceil$  and  $Q_2 = \lceil \log_2(n_2 + 1) \rceil$ ). In formula (43) the first transformation produces the sum and difference of occupation number pairs  $(f_p, f_q)$  and  $(f_r, f_s)$ ,

$$\Sigma_1 = f_q + f_p, \quad (44)$$

$$\Delta_1 = f_q - f_p, \quad (45)$$

$$\Sigma_2 = f_s + f_r, \quad (46)$$

$$\Delta_2 = f_s - f_r, \quad (47)$$

and the second transformation in (43) produces sum and difference of the first and third registers denoted  $\Sigma_1$  and  $\Sigma_2$  respectively,

$$\Sigma = \Sigma_2 + \Sigma_1, \quad (48)$$

$$\Delta = \Sigma_2 - \Sigma_1. \quad (49)$$

The whole Trotter step (35) is represented by a quantum circuit model in Fig. 4 and the particular implementation of the ASG gate is discussed in detail in Chapter 2.3 of the Supplementary Information. Note that the ASG gate can be realized by  $\mathcal{O}(Q)$  elementary gates and (depending on a particular realization) with 0 to  $Q$  working qubits. The existence of the ASG gate is obvious from the fact that from the combination of the sum and difference of the two input integers, the input integers can be unambiguously deduced. The ASG gate outputs for the ancilla registers  $|a_i\rangle$  different from zeros are irrelevant.



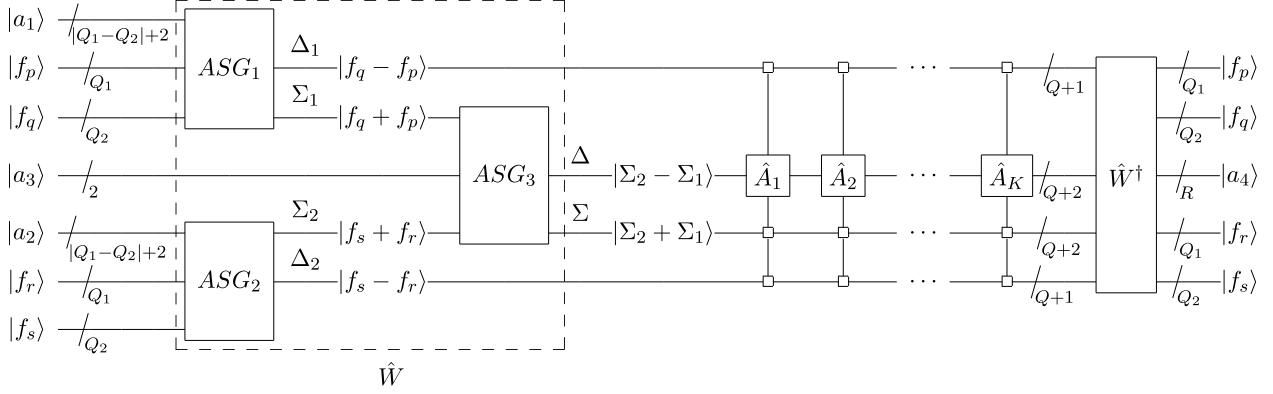


Figure 4: The quantum circuit implementing a single Trotter step (boson-boson interaction, see Eq. (35), (36) and (39)). The  $\hat{A}_i$   $Q + 2$  qubit gates are controlled by  $i$ -specific  $Q + 1$ ,  $Q + 2$  and  $Q + 1$  bit sequences, quantum circuit corresponding to them is presented in Fig. 5 with one additional working qubit increasing the number of qubits  $\hat{A}_i$  operates on to  $Q + 3$ . The gate labeled ASG is the Adder-Subtractor Gate realizing the simultaneous addition (sum) and subtraction of two binary represented integers. The different indices for ASG gates corresponds to different ordering of outputs and inputs. The  $|Q_1 - Q_2| + 2$ -qubit kets  $|a_1\rangle$  and  $|a_2\rangle$  are initially set to zero ( $|0\rangle$ ) and correspond to the necessity to pad the input integer with less bits with  $|Q_1 - Q_2|$  zeros to match the number of bits of the greater input integer prior the particular logical operation, one carry bit is needed for the output integer corresponding to the sum and one extra bit (sign bit) is needed for the output integer corresponding to the difference. Similarly, the ket  $|a_3\rangle$  is a 2-qubit initially set to zero ( $|00\rangle$ ) to provide the most significant bit for the sum  $\Sigma$  and the sign bit for the difference  $\Delta$ . The ket  $|a_4\rangle$  is a  $R = 2|Q_1 - Q_2| + 6$  register for the recovery of all working qubits.

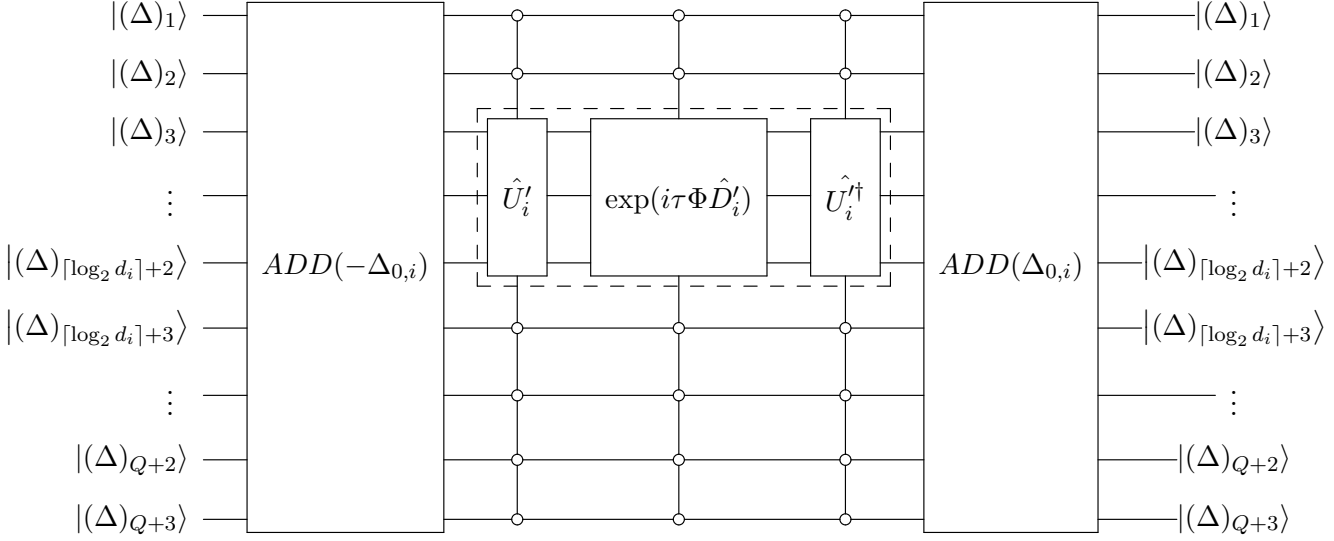


Figure 5: The quantum circuit representing the action of the gate  $\hat{A}_i$  (which occurs in Fig. 4 and equations (41) and (42)) on its target quantum register  $\Delta$  padded by one ancilla qubit  $(\Delta)_{Q+3}$  needed for ADD gate operation. The Q+3 qubit gate  $\text{ADD}(a)$  adds a constant integer  $a = \pm\Delta_{0,i}$  to the input quantum register producing the output quantum register. The ADD gate is based on the generalized  $\Phi$  ADD gate (operating in  $\mathcal{O}(1)$  time, see the Fig. 4 on the page 654 of<sup>67</sup>) inserted between the forward and backward Quantum Fourier Transforms (operating in  $\mathcal{O}(Q \log Q)$  time each). The value  $\Delta_{0,i}$  corresponding to the  $i$ -th subspace (in the decomposition (39)) is the smallest value of  $\Delta$  corresponding to any vector in that subspace and is to be precomputed classically for each  $i$  in  $\{1, 2, \dots, K\}$ . The primes correspond to the fact that the operators now act on different subspaces. In the special case of one dimensional subspaces ( $d_i = 1$ ),  $\hat{U}_i'$ ,  $\exp(i\tau\Phi\hat{D}_i')$  and  $\hat{U}_i'^{\dagger}$  gates have 0 qubit target register and are therefore equal to multiply controlled phase-shifts. Since the corresponding phase is  $1 = \exp(0)$  for all of them, they can be omitted from the quantum circuit.

The transformation (43) needs  $2|Q_1 - Q_2| + 4$  ancillary qubits for the first part and another 2 ancillary qubits for the second part. Therefore the first and the last quantum registers (storing the values of  $\Delta$  and  $\Sigma$  respectively) have a size  $\max(Q_1, Q_2) + 2$  qubits while the middle quantum registers (storing the values of  $\Delta_1$  and  $\Delta_2$ ) of  $\max(Q_1, Q_2) + 1$  qubits. In the following text,  $Q \equiv \max(Q_1, Q_2)$ . The number of single qubit gates and CNOTs for the transformation (43) scales as  $\mathcal{O}(Q)$  if the algorithm presented in<sup>68</sup> is used (with another  $Q + 1$  working qubits) or as  $\mathcal{O}(Q \log Q)$  (but with no need for further working qubits) if the algorithm exploiting QFT<sup>69, 70</sup> is employed. Each  $\hat{U}_i$  quantum gate acts on the target register which is subregister of the first register in the last part of (43), storing the value of  $\Delta$  and is multiply controlled by other qubits representing the ket  $|\Delta, \Delta_1, \Delta_2, \Sigma\rangle$ . Multiply controlled quantum gates can be decomposed into the bare quantum gate acting on the target register and either  $\mathcal{O}(Q)$  (1-qubit and CNOT) gate cost with using  $3Q + 2$  working ancillary qubits or  $\mathcal{O}(Q^2)$  gate cost without any working ancillary qubits (for the algorithm see<sup>1</sup> on pages 183 and 193 respectively, the variant with ancillary qubits is also mentioned in<sup>71</sup>). The action of  $\hat{A}_i$  gate from Fig. 4 and equations (41) and (42) is described in the quantum circuit in Fig. 5. The bare quantum gate from Fig. 5,  $\hat{U}'_i$ , acting on the target register ( $2^{\lceil \log(d) \rceil}$ -dimensional subspace) can be decomposed (via Quantum Shannon Decomposition (QSD),<sup>72</sup>) into  $\mathcal{O}(d^2)$  elementary quantum gates. Neglecting the contribution of gates acting on the controlling register which scales as  $\mathcal{O}(M_{S,0}Q^2) = \mathcal{O}(x^2 y \log^2(x + 1))$  in the worst case, the formula for  $N_{\text{gates}}(n, m)$  (31) is derived as  $M_{S,2}$ . The diagonal bare quantum gate  $\exp(i\tau\Phi\hat{D}'_i)$  can be decomposed into the 1-qubit gates and CNOTs at most with the same effort as  $\hat{U}'_i$  as further discussed in the Supplementary Information (Chapter 2.4.). It is important to note, that the classical pre-processing - diagonalization of  $\hat{V}$  and QSD of the corresponding  $\hat{U}_i$  operators needs to be done just once (for e.g.  $p = 1, q = 2, r = 3, s = 4$ ) before the quantum algorithm is started, then for each elementary Trotter term (35) the sequence of quantum gates differs just by addressing different quantum registers (no longer  $p = 1, q = 2, r = 3, s = 4$ ) and by different value of  $\Phi = V_{pqrs}$  as term in phase-parameter in  $\exp(i\tau\Phi\hat{D})$  diagonal operator from lemma (36).

## Acknowledgement

This work has been supported by the Grant Agency of the Czech Republic - GAČR (203/08/0626) and by the Charles University project “Student research in biophysics and chemical physics” (SVV 260214).

## References

- [1] M. A. Nielsen and I. L. Chuang, *Quantum Computation and Quantum Information* (Cambridge University Press, 2000).
- [2] S. Lloyd, Science **273**, 1073 (1996).
- [3] C. Zalka, Proc. R. Soc. London Ser. A **454**, 313 (1998).
- [4] G. Ortiz, J. E. Gubernatis, E. Knill, and R. Laflamme, Phys. Rev. A **64**, 022319 (2001).
- [5] R. Somma, G. Ortiz, J. E. Gubernatis, E. Knill, and R. Laflamme, Phys. Rev. A **65**, 042323 (2002).
- [6] D. S. Abrams and S. Lloyd, Phys.Rev.Lett. **79**, 2586 (1997).

- [7] D. S. Abrams and S. Lloyd, Phys.Rev.Lett. **83**, 5162 (1999).
- [8] E. Ovrum and M. Hjorth-Jensen, arXiv:quant-ph/0705.1928v1 (2007).
- [9] R. P. Feynman, Int. J. Theor. Phys. **21**, 467 (1982).
- [10] Manin, Yu. I. (1980) (in Russian). Vychislimoe i nevychislimoe [Computable and Noncomputable]. Sov.Radio. pp. 1315.
- [11] A. Aspuru-Guzik, A. D. Dutoi, P. J. Love, and M. Head-Gordon, Science **309**, 1704 (2005).
- [12] H. Wang, S. Kais, A. Aspuru-Guzik, and M. R. Hoffmann, Phys. Chem. Chem. Phys. **10**, 5388 (2008).
- [13] J. D. Whitfield, J. Biamonte, and A. Aspuru-Guzik, Mol. Phys. **109**, 735 (2011).
- [14] L. Veis and J. Pittner, J. Chem. Phys. **133**, 194106 (2010).
- [15] L. Veis *et al.*, Phys. Rev. A **85**, 030304 (2012).
- [16] I. Kassal, S. P. Jordan, P. J. Love, M. Mohseni, and A. Aspuru-Guzik, Proc. Natl. Acad. Sci. **105**, 18681 (2008).
- [17] I. Kassal and A. Aspuru-Guzik, J. Chem. Phys. **131**, 224102 (2009).
- [18] I. Kassal, J. D. Whitfield, A. Perdomo-Ortiz, M. H. Yung, and A. Aspuru-Guzik, Annu. Rev. Phys. Chem **62**, 185 (2011).
- [19] M.-H. Yung, J. D. Whitfield, S. Boixo, D. G. Tempel, and A. Aspuru-Guzik, Adv. Chem. Phys. **154**, 67 (2014).
- [20] L. Veis and J. Pittner, Adv. Chem. Phys. **154**, 107 (2014).
- [21] B. P. Lanyon *et al.*, Nat. Chem. **2**, 106 (2010).
- [22] J. Du *et al.*, Phys. Rev. Lett. **104**, 030502 (2010).
- [23] Z. Li *et al.*, Sci. Rep. **1**, 88 (2011).
- [24] D. Lu *et al.*, Phys. Rev. Lett. **107**, 020501 (2011).
- [25] B. P. Lanyon *et al.*, Science **334**, 57 (2011).
- [26] A. Peruzzo *et al.*, Nat. Commun. **5**, 4213 (2013).
- [27] N. C. Jones *et al.*, New J. Phys. **14**, 115023 (2012).
- [28] M. Tachikawa, K. Mori, H. Nakai, and K. Iguchi, Phys. Lett. **290**, 437 (1998).
- [29] H. Nakai, Int. J. Quant. Chem. **86**, 511 (2002).
- [30] H. Nakai and K. Sodeyama, J. Chem. Phys. **118**, 1119 (2003).
- [31] H. Nakai, Int. J. Quant. Chem. **107**, 2849 (2007).
- [32] H. Nakai, M. Hoshino, K. Miyamoto, and S. Hyodo, J. Chem. Phys. **122**, 164101 (2005).

- [33] M. Hoshino and H. Nakai, J. Chem. Phys. **124**, 194110 (2006).
- [34] K. Miyamoto, M. Hoshino, and H. Nakai, J. Chem. Theory Comput. **2**, 1544 (2006).
- [35] R. B. Griffiths and Chi-Sheng Niu, Phys. Rev. Lett. **76**, 3228 (1996).
- [36] A. Szabo and N. Ostlund, *Modern Quantum Chemistry: Introduction to Advanced Electronic Structure Theory* (Dover Publications, 1996).
- [37] N. Hatano and M. Suzuki, Quantum annealing and other optimization methods, in *Lecture Notes in Physics*, chap. Finding Exponential Product Formulas of Higher Orders, Springer, Heidelberg, 2005.
- [38] P. Jordan and E. Wigner, Z. Phys. A **47**, 631 (1928).
- [39] S. B. Bravyi and A. Y. Kitaev, Ann. Phys. **298**, 210 (2002).
- [40] J. T. Seeley, M. J. Richard, and P. J. Love, J. Chem. Phys. **137**, 224109 (2012).
- [41] B. Toloui and P. J. Love, arXiv:1312.2579 (2013).
- [42] D. Wecker, B. Bauer, B. K. Clark, M. B. Hastings, and M. Troyer, Phys. Rev. A **90**, 022305 (2014).
- [43] D. Poulin *et al.*, Quantum Information and Computation **15**, 0361 (2015).
- [44] J. R. McClean, P. J. Love, and A. Aspuru-Guzik, J. Phys. Chem. Lett. **5**, 4368 (2014).
- [45] L. Veis and J. Pittner, J. Chem. Phys. **140**, 214111 (2014).
- [46] J.-S. Xu *et al.*, Nat. Photon. **8**, 113 (2014).
- [47] M.-H. Yung *et al.*, Sci. Rep. **4**, 3589 (2013).
- [48] A. D. Bochevarov, E. F. Valeev, and C. D. Sherrill, Mol. Phys. **102**, 111 (2004).
- [49] W. P. Webb, T. Iordanov, and S. Hammes-Schiffer, J. Chem. Phys. **117**, 4106 (2002).
- [50] M. Born and R. Oppenheimer, Ann. Phys. **84**, 457 (1927).
- [51] H. Nakai, K. Sodeyama, and M. Hoshino, Chem. Phys. Lett. **345**, 118 (2001).
- [52] M. Hoshino, H. Nishizawa, and H. Nakai, J. Chem. Phys. **135**, 024111 (2011).
- [53] H. Nishizawa, M. Hoshino, Y. Imamura, and H. Nakai, Chem. Phys. Lett. **521**, 142 (2012).
- [54] H. Nishizawa, Y. Imamura, Y. Iwabata, and H. Nakai, Chem. Phys. Lett. **533**, 100 (2012).
- [55] J. D. Biamonte, V. Bergholm, J. D. Whitfield, J. Fitzsimons, and A. Aspuru-Guzik, AIP Advances **1**, 022126 (2011).
- [56] M. Stanke, D. Kędziera, S. Bubin, M. Molski, and L. Adamowicz, The Journal of Chemical Physics **128**, 114313 (2008).
- [57] S. Bubin, F. Leonarski, M. Stanke, and L. Adamowicz, Chemical Physical Letters **477**, 12.16 (2009), bubin's publications are in <http://neon.phy.vanderbilt.edu/docs/publications>.

- [58] K. Pachucki and J. Komasa, The Journal of Chemical Physics **130**, 164113.164124 (2009).
- [59] J. Komasa *et al.*, Journal of Chemical Theory and Computation **7**, 3105.3115 (2011).
- [60] M. Weitz *et al.*, Physical Review A **52**, 2664.2681 (1995).
- [61] J. Liu *et al.*, The Journal of Chemical Physics **130**, 174306.174314 (2009).
- [62] G. D. Dickenson *et al.*, Phys. Rev. Lett. **110**, 3601.3605 (2013).
- [63] J. Lloyd-Williams, A vmc study of the isotopologues of  $h_2$  and  $h_2^+$ , presentation for Electronic Structure Discussion Group at University of Cambridge (1994).
- [64] W. Kolos and L. Wolkiewicz, The Journal of Chemical Physics **49**, 404.410 (1968).
- [65] M.-C. Chuang and R. N. Zare, Journal of Molecular Spectroscopy **121**, 380.400 (1987).
- [66] T. Hagerup and C. Rüb, Information Processing Letters **33**, 305 (1990).
- [67] A. Pavlidis and D. Gizopoulos, Quantum Information and Computation **14**, 649.682 (2014).
- [68] V. Vedral, A. Barenco, and A. Ekert, Physical Review A **54**, 147 (1996).
- [69] G. Florio and D. Picca, arXiv:quant-ph/0403048 (2004).
- [70] L. Ruiz-Perez and J. C. Garcia-Escartin, arXiv:quant-ph/1411.5949 (2014).
- [71] S. S. Agaian and A. Klappenecker, Quantum computing and a unified approach to fast unitary transforms, in *SPIE Proceedings, Vol 4667, Algorithms I, Image Processing: Algorithms and Systems, 1*, pp. 1–11, , 2002, SPIE.
- [72] V. V. Shende, S. S. Bullock, and I. L. Markov, IEEE Trans. on Computer-Aided Design **25**, 1000 (2006).